VII International Conference on Computational Methods in Marine Engineering
MARINE 2017
M. Visonneau, P. Queutey and D. Le Touzé (Eds)

A NUMERICAL STUDY OF ADDED RESISTANCE, SPEED LOSS AND ADDED POWER OF A SURFACE SHIP IN REGULAR HEAD WAVES USING COUPLED URANS AND RIGID-BODY MOTION EQUATIONS

MARINE 2017

SHAWN ARAM* AND SUNG-EUN KIM**

Naval Surface Warfare Center, Carderock Division
West Bethesda, MD, USA
e-mail: shawn.aram@navy.mil*; sungeun.kim@navy.mil**

Key words: URANS, 6-DOF ship motion, added resistance, added power, head waves

Abstract. Coupled solutions of two-phase Unsteady Reynolds-Averaged Navier-Stokes equations (URANS) and six degrees-of-freedom (6-DOF) rigid-body motion (RBM) equations are pursued to compute ship's speed loss and added power for a self-propelling ship in regular head sea. A case study is presented for a 1/49 scale model of the ONR Tumblehome (ONRT) (Model 5613) which was tested in the towing tank of the Iowa Institute of Hydraulic Research (IIHR). The computations were carried out for various combinations of towed and self-propelled conditions, and in calm water and regular head waves with a range of wave length and amplitude. The case study demonstrates that the coupled URANS and RBM solution approach can predict added resistance, speed loss and added power of a ship cruising in head waves with commendable accuracy and shed light on the complex interactions among the ship, propeller, waves and flow-fields.

1 INTRODUCTION

Ship's resistance and engine power to sustain ship's speed in seaways are augmented due to complex non-linear interactions between the ship and the ambient sea (waves). Ship designers, in early design stage, use an *ad hoc* "sea margin" to account for the effects of seaways in selecting propeller and engine. A numerical tool capable of accurately predicting added resistance and power of a ship cruising in waves would greatly help select its powering (margin) requirement and determine the optimal operating point that can maximize the energy efficiency.

For seakeeping analysis, strip theory-based methods have long been used. More recently, nonlinear time-domain three-dimensional (3D) panel methods have started being used widely [1]. A more physics-based avenue to seakeeping analysis is offered by coupled solutions of two-phase unsteady Reynolds-Averaged Navier-Stokes equations and six degrees-of-freedom rigid-body motion (RBM) equations [2, 3, 4]. The URANS approach also avails itself of including the effects of propulsors, either explicitly or approximately. By accounting for all the nonlinear effects in hydrodynamic forces and moments and the resulting ship motions, and the effects of fluid viscosity and turbulence, the coupled URANS-RBM method is believed not only able to predict added resistance and speed loss more accurately but also to provide valuable insights into the physical mechanisms underlying added resistance and power.

The objectives of this study are:

- To validate a coupled URANS-RBM solver developed for high-fidelity prediction of added resistance, speed loss and added power on ships cruising in regular head sea.
- To conduct a detailed analysis of the interactions among ship hull, propeller and waves for a 1/49 scaled model of the ONR Tumblehome (ONRT) (Model 5613) in order to shed light on the physical mechanisms leading to added resistance, speed loss and added power

2 SHIP MODEL

The ONR Tumblehome (ONRT) model 5613, shown in Figure 1, is considered for the present study. It is a fully appended 1/49 scale model equipped with a skeg, bilge keels, twin rudders, shafts and two 4-bladed propellers mounted with shaft brackets. Each propeller has 4 fixed-pitch type blades with inward direction of rotation (view from bow/stern). The main particulars of the ship are given in Table 1.

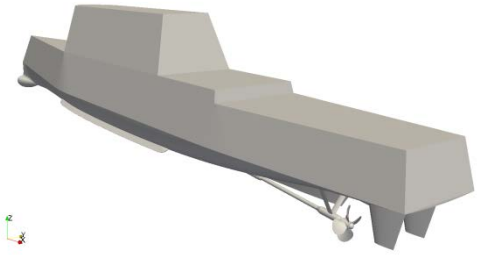

Figure 1: ONR Tumblehome (ONRT) model 5613

Table 1: Particulars of ONRT model scale hull

Main Particulars	Model Scale
Displacement, Δ (kg)	72.6
Waterline Length, L (m)	3.147
Waterline Beam, B_{WL} (m)	0.384
Draft, T (m)	0.112
Wetted Surface Area, S (m_2)	1.5
L_{CB} (m aft of FP)	1.625
V_{CG} (m from keel)	0.156
Yaw Inertia (K_{yy}/L)	0.246
Propeller Diameter, D_p (m)	0.1066
Propeller Shaft Angle (deg)	5

Free-running tests of the hull at various maneuvering conditions in calm water and regular waves were performed at the IIHR Wave Basin Facility [5, 6]. The experimental data are used to validate the predictions in this paper.

3 COMPUTATIONAL METHOD

3.1 CFD Solver – NavyFOAM

All the URANS-based simulations were conducted using an in-house CFD framework, NavyFOAM. NavyFOAM is a suite of CFD codes developed using OpenFOAM®, an open-

source continuum mechanics software library written in C++. OpenFOAM makes use of object-oriented programming techniques offered by the C++ language that allow one to maximize code re-use, adopt layered development, expedite building top-level applications, and make runtime-selection of numerical schemes, solution algorithms, physical models, and file I/O. NavyFOAM offers additional libraries in areas such as discretization schemes and physical models. Several top-level solvers for single- and multi-phase flows have also been added in NavyFOAM aiming at marine applications including underwater vehicles, surface ships, and propulsors [7].

The Navier-Stokes solvers in NavyFOAM employ a cell-centered finite-volume method based on a multi-dimensional linear reconstruction scheme that permits use of arbitrary polyhedral cells. The free surface (air-water interface) is resolved by a two-phase, single-fluid Volume-Of-Fluid (VOF) method [8]. Among the schemes offered in NavyFOAM to discretize the advection term in the volume-fraction equation, the modified high resolution interface capturing (MHRIC) scheme [8] is employed in the current study. The advection term in the momentum equation is discretized using the 2^{nd}-order upwind scheme with skewness correction employed for the diffusion term.

The continuity, momentum, volume-of-fluid and turbulence equations are solved implicitly in a segregated manner. The 2^{nd}-order backward-differencing scheme is used for temporal discretization. The SST k-ω model is employed to model the turbulence.

The "rigid-body mesh" option in NavyFOAM is used to model 3-DOF (straight ahead self-propulsion, free to surge, heave and pitch) motions of the ONRT model. The coupled solutions of the URANS and 6-DOF motion equations are obtained using a predictor-corrector-based, iterative algorithm that not only preserves a formal 2^{nd} -order temporal accuracy, but ensures stability of the coupled solutions. The tight coupling in the solution algorithm is achieved by nested loops where each coupling loop contains an outer iterative loop for the flow equations. Three coupling loops and two outer iterations are used in this study.

The effects of propellers could be modeled in NavyFOAM using one of the following techniques:

- Direct method based on the Generalized Grid Interface (GGI) technique, in which the actual propeller rotation is modeled. The GGI, which is an efficient and scalable algorithm for sliding grids, allows for a time-accurate solution to be obtained for propeller-hull interactions. This method uses a special algorithm to compute weights for solution interpolation between two overlapping non-conformal surfaces. It should be pointed out that this method is computationally expensive due to the very small time-step size necessary to resolve the time scales associated with propeller-hull interactions.
- Body-force model, where the propeller geometry is excluded from the model. Given the orientation and location of the propeller, the surrogate model dynamically updates the thrust and torque using the characteristics (K_T, K_Q vs. J) and the ship speed or local inflow velocity evaluated at each time instant. Variation in thrust and torque with the average in-flow rate and impeller RPM (K_T and K_Q vs. J) are derived from available propeller performance data. Using the body-force model, a volumetric body-force which represents the effect of actual rotating propeller is distributed at the location of propeller. The Hoekstra's actuator disk model [9] is adopted in NavyFOAM to model the radial distribution of body force.

Both the direct method and the body-force model were used in this study to model the thrust generated by propellers and to evaluate the accuracy and efficiency of each method.

A wave-making library modified from the Waves2Foam package and integrated into NavyFOAM, was used to generate a single 1^{st}-, 2^{nd}- and 5^{th}- order Stokes waves. It also supports a wave relaxation zone, within which the analytical flow and wave fields (flow velocity and volume-fraction) are implicitly blended with the solutions to the transport equation, using a predefined blending function (exponential function in this study). The computational time can be saved by using a wave-making zone along with the wave boundary condition specified at the inlet of the computational domain. The wave damping zone can be used near the outlet of the domain to minimize the wave reflections from the exit boundary. This is achieved by adding an artificial damping body-force term to the momentum equation. As a result, the flow velocity at the end of the damping zone tends to vanish, and the free surface recovers its calm-water position.

3.2 Computational Domain and Grids

The computational domain extends 1.5L forward of the forward perpendicular, 3.0L aft of the aft perpendicular, 2.0L to the side, L from top to waterline and 1.5L from waterline to bottom, where L is the waterline length.

HEXPRESS^{TM}, a commercial meshing software package from NUMECA, was used to generate non-conformal body-fitted full hexahedral unstructured meshes. Quadrilateral elements were predominantly used to construct the hull surface in combination with the local refinements to properly capture the sharp edges (see Figure 2). The largest cell size (edge length) of the background grid is 0.75m (~L/4) in all three directions. Figure 3 shows the grid distribution on the centerline plane. The grid nodes are uniformly distributed along streamwise (x) and vertical (z) directions within the wave relaxation zone which extends 1.0L from the inlet boundary. Extensive grid sensitivity studies with a 2D wave tank and the Korean Container Ship (KCS) hull in regular waves with various wave slopes were conducted to determine a grid resolution required to accurately resolve the waves. The grid nodes are stretched along the x-direction inside the damping zone in order to damp the wave reflections at the outlet boundary. The "rigid-body dynamic mesh" method, in which the entire grid moves (translates and rotates) with the body, requires a band of the free-surface refinement zone to be sufficiently large not to lose the grid resolution near the upstream inlet boundary. The choice of the band-width depends on the incoming wave height as well. The near-wall resolutions are commensurate with the wall functions. On the hull surface, y^+ ranges from 50 – 70. The total number of cells for the case of body-force model varies between 5.2 million and 6.34 million elements, depending on the wave slope.

Figure 4 shows the surface grid on the propeller blades and the volume grid in the cylindrical rotating zone surrounding the propeller. As shown, the grid properly resolves the blades tips and edges. The total number of cells in the rotating zone is 1.5 million. The total cell count for the entire computational domain including the propeller and hull grids is 7.3 million.

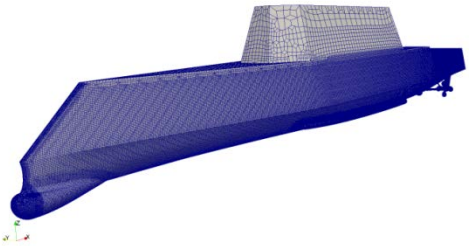

Figure 2: Quadri-lateral surface grid elements on the ONRT hull

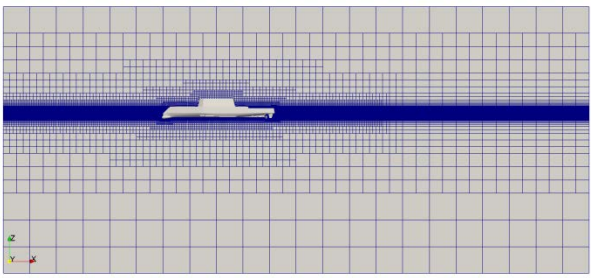

Figure 3: Hexahedra-dominant grid on the centerline of the computational domain

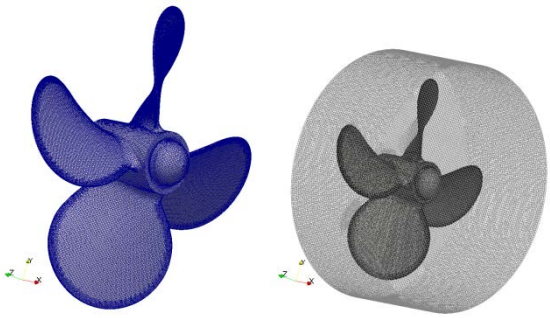

Figure 4: Surface and volume grids for the ONRT propeller

The sensitivity of the computational results to the grid resolution was also examined by doubling the grid resolution in all three directions at the critical zones including near hull surface, propeller (body-force model), air-water interface, and wake regions. The total number of elements of this refined grid is 24.5 million.

3.3 Simulation Conditions

Table 2 summarizes the simulation conditions considered in this study. In all our computations, the ship was set free to surge, heave and pitch (3-DOF), but was constrained in sway and yaw. It should be noted that, in the model test, the model ship was set free to yaw, and the rudder angle was constantly adjusted using a controller to keep the model in a straight course. The self-propulsion simulations were performed first in calm-water to provide a reference condition for the subsequent added-power and added-resistance studies (Cases 1 and 2). The computational results (ship's speed, sinkage and trim) were compared against the experimental data obtained at the IIHR's Wave Basin Facility [5, 6]. Both the body-force model and the direct method were used to simulate the self-propulsion conditions at a constant propeller rotational speed of 538 RPM (Case 1). The simulation with a variable

RPM for the target ship speed of 1.11 m/s ($Re = 3.4 \times 10^6$, Fr = 0.2) was also performed using the body-force model (Case 2) to be used for the added power analysis. The resistance prediction of the ship towed in calm water was conducted as well for use in the propeller-hull interaction study (Case 3).

To represent regular head seas, three different wave-lengths of λ/L=0.5, 1.0 and 2.0 at a constant wave-slope of h/L=0.02 were considered. Thus, the corresponding wave-height also increases with the wave-length. Cases 4 to 6 were to study the ship's speed loss in head waves at a fixed propeller speed (538 RPM). Except for Case 5 (λ/L=1.0), the body-force model was exclusively used to simulate the propeller effects. The speed-loss predictions for Case 5 (λ/L=1.0) were validated against the experimental data of Sanada et al. [5, 6] using both the body-force model and direct method for propeller.

For the added-power study, a Proportional Integral Derivative (PID) controller was used to maintain the target ship speed of 1.11 m/s as reported in the IIHR's experiments for the calm water condition (Case 1), by varying the propeller RPM. Similar to the speed-loss study, the added power was computed for three wave lengths of λ/L=0.5, 1.0 and 2.0 (Case 7-9). Resistance predictions of the hull at these wave conditions (case 10-12) were also performed to determine the added resistance due to waves and to aid the propeller-hull interaction analyses for both constant and variable propeller RPM conditions. Each of Cases 10 to 12 ran with two different ship speeds: (1) the target speed of 1.11m/s (for the added resistance and added power study), (2) the ship speed determined by the self-propulsion simulation at constant propeller RPM of 538 (for the speed loss study).

Table 2: Simulation conditions

Case no.	Wave condition	Motion condition	RPM	Propeller action
1	Calm water	Self-prop	538	on* (body-force &direct)
2	Calm water	Self-prop	Var	On
3	Calm water	Tow	-	Off
4	Reg. wave λ/L=0.5	Self-prop	538	On
5	Reg. wave λ/L=1.0	Self-prop	538	on* (body-force & direct)
6	Reg. wave λ/L=2.0	Self-prop	538	On
7	Reg. wave λ/L=0.5	Self-prop	Var	On
8	Reg. wave λ/L=1.0	Self-prop	Var	On
9	Reg. wave λ/L=2.0	Self-prop	Var	On
10	Reg. wave λ/L=0.5	Tow (2 speeds)	-	off
11	Reg. wave λ/L=1.0	Tow (2 speeds)	-	off
12	Reg. wave λ/L=2.0	Tow (2 speeds)	-	off

* denote cases where the propeller was modeled using both the direct method and the body-force approach

4 RESULTS AND DISCUSSION

4.1 Calm Water Condition

The predicted ship speed, sinkage and trim in calm water (Case 1) at the constant propeller RPM are compared with the experimental data in Table 3. The prediction of the ship speed using the body-force model is in excellent agreement with the measurement (0.5% difference), while the direct method under-predicted it by 5.0%. This may seem somewhat puzzling, inasmuch as one would expect better prediction from the direct method. At this point, we can only surmise that the experimental uncertainties arising from the use of a fairly small model (model ship length of 3.15 m and propeller diameter of 0.1 m), the effects of yaw allowed in the experiment, and modeling error could potentially be attributable to the discrepancy. Thus, the seemingly excellent prediction by the body-force model may well be fortuitous. The sinkage and trim predictions seem reasonable, although the percentage differences from the measurements are quite large due to the very small values of the trim and sinkage.

Table 3: Experimental and CFD prediction for self-propulsion in calm water condition at a fixed propeller RPM

	Speed (m/s)	Sinkage (m)	Trim (deg)
CFD-Body-Force Model	1.105	0.0015	-0.120
CFD-Direct Method	1.052	0.0013	-0.093
EFD (Sanada et al.[5,6])	1.11	0.0023	-0.039

Another way of validating the prediction for the IIHR's experiment in calm-water condition is using the PID controller to adjust the propeller RPM to maintain the target ship speed of 1.11 m/s (Case 2). The present computation with the body-force model showed that the required RPM is found to be 541, which is slightly higher (0.5%) than the RPM used in the experiment.

4.2 Regular Wave Conditions

4.2.1 Added Resistance

Before presenting the speed loss and added power, the added resistance due to the head waves was computed using the results of the computations carried out for the towed conditions without the propellers (Cases 3, 10, 11, 12). Table 4 summarizes the results.

Table 4: Added resistance of ONRT due to waves towed at a constant speed of 1.11 m/s (Fr = 0.2)

Wave condition	$\Delta\overline{C_T}$ ($\times 10^3$)
λ/L=0.5	0.375
λ/L=1.0	4.363
λ/L=2.0	1.884

4.2.2 Speed Loss

The computations were carried out with three different wave lengths (and heights) to predict the speed loss. Figure 5 shows the time histories of the ship speed, sinkage and trim predicted for the case of λ/L=1.0 and h/L=0.02 (Case 5) with the propeller operating at a fixed (538) RPM, along with the experimental data. Note that the ship speed plotted here was made dimensionless using the ship speed in calm water (denoted "V" in the plot). The wave encounter period, T_e, is used to non-dimensionalize time throughout this paper. The time-averaged ship speed is seen to be slightly under-predicted closely by both the body-force

method (1.7%) and the direct method (2.4%), respectively. However, the oscillation amplitude of the measured ship speed is almost twice as large as the predictions. The cause for the much larger oscillation amplitude of the measured ship speed is not clear, other than the plausible effects of the yaw motion of the ship model. Interestingly, the oscillation amplitude of the ship speed is also under-predicted by all others who tacked this case [5, 6, 10, 11]. The predicted amplitudes of the ship motion (heave and pitch) are in close agreement with the measurements, being slightly under-predicted.

The grid sensitivity of the predictions was also studied using the body-force model. Figure 6 shows the time histories of the ship speed, sinkage and trim obtained using 7.3 million cell (coarse grid) and 24.5 million cell (fine grid) grids. The predictions with both grids almost fall on top of each other, which indicate that the coarse mesh practically gives grid-convergent solutions.

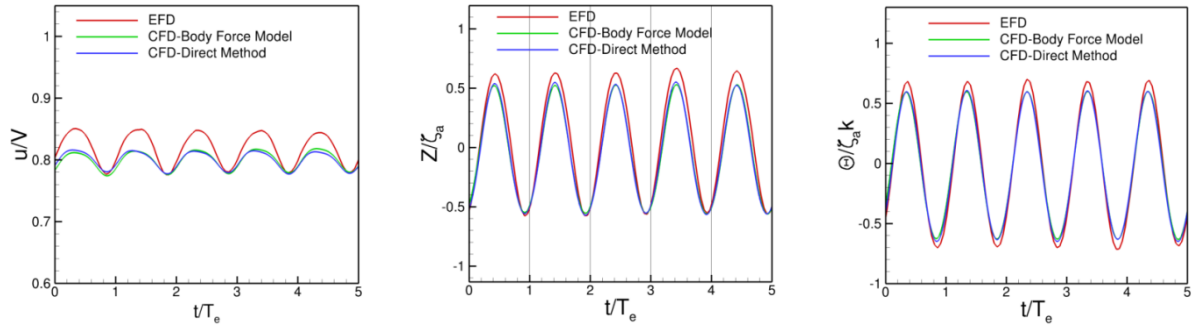

Figure 5: Comparison of time histories ship speed, sinkage and trim in regular waves at λ/L=1.0 and h/L=0.02 conditions between CFD and EFD at fixed propeller RPM of 538

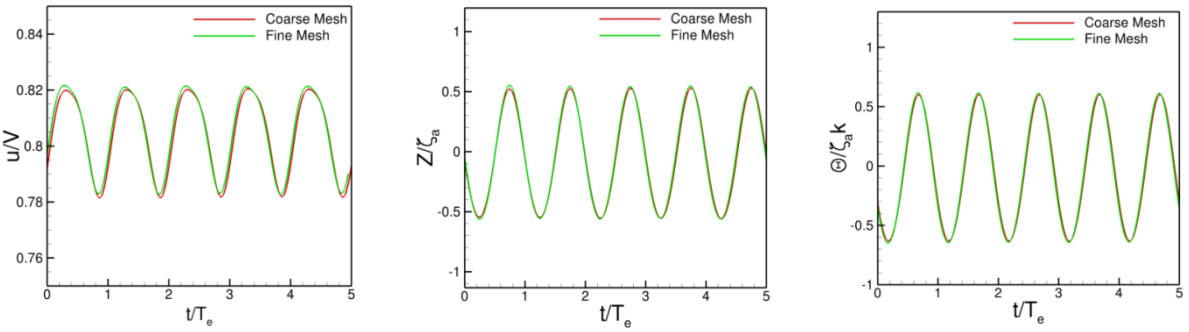

Figure 6: Grid sensitivity study for self-propulsion simulations in regular waves at λ/L=1.0, h/L=0.02 conditions and fixed propeller RPM of 538

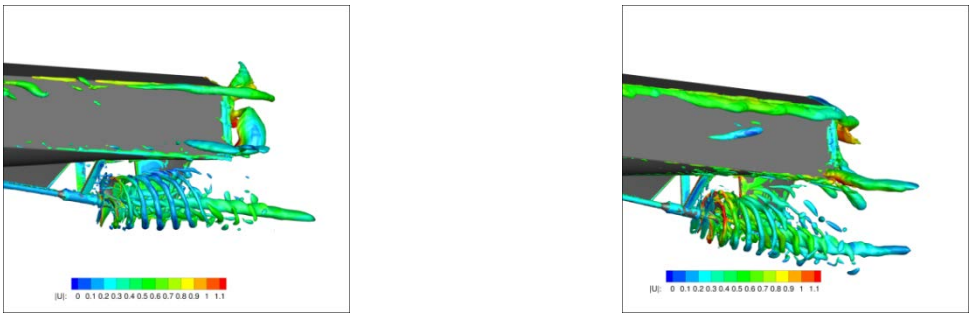

Figure 7: Iso-surface of Q (the second invariant of velocity deformation tensor) colored by the flow velocity magnitude at the stern region at minimum (left figure) and maximum surge speed (right figure)

The iso-surfaces of the Q colored by the velocity magnitude are shown in Figure 7 near the ship's stern at two time instants corresponding to the moments when the ship attains the minimum and the maximum surge speed, respectively. The main flow features expected at the ship's stern, such as the hub vortices and blade-tip vortices from the propeller are captured. It is also seen that the velocity magnitude along the tip vortices is noticeably greater at the maximum surge velocity than at the minimum surge velocity.

We summarized in Table 5 the hull axial force and its breakdowns to the pressure and frictional components for the calm-water and the wave conditions. Note that the hull forces were non-dimensionalized using the time-averaged ship speeds obtained for individual wave conditions. Also note that the hull force was computed by integrating the pressure and shear stresses over the hull with the propeller operating at a constant RPM. Thus, the hull axial force reported here accounts for the effects of the propeller. As can be seen, it is the pressure force component that is more affected by the change in the wave length and height. Both the total hull force along with its pressure and viscous contributions are the greatest at λ/L=1.0 ("resonance condition"), among all the flow conditions studied here. Figure 8 shows the time histories of the non-dimensional pressure and viscous components of the hull axial force at the calm water and wave conditions. The oscillation amplitudes of the pressure force coefficient increase with the wave length and height. The oscillation amplitudes of the viscous force coefficient at λ/L=1.0 and 2.0 are substantially larger than that for λ/L=0.5 presumably due to the changes in the wetted surface area. The oscillation amplitude of the pressure force coefficient is much larger than the viscous force coefficient at all wave conditions.

Table 5: Time average of non-dimensional pressure and viscous components and total of hull axial force coefficients ($\times 10^3$) at calm water and wave conditions and a fixed propeller RPM of 538

Wave condition	$\overline{C}_{Hull,p}$	$\overline{C}_{Hull,vis}$	$\overline{C}_{tot}$
Calm water	0.813	3.6	4.413
λ/L=0.5	1.340	3.996	5.336
λ/L=1.0	5.745	4.804	10.549
λ/L=2.0	3.23	4.347	7.577

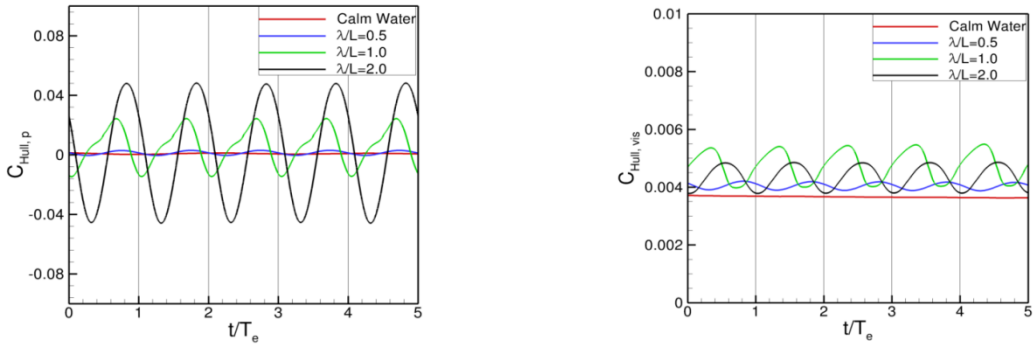

Figure 8: Time histories of non-dimensional pressure and viscous components of the axial hull force in head waves at λ/L=0.5, 1.0, 2.0, h/L=0.02 conditions and fixed propeller RPM of 538

The time histories of non-dimensional sinkage and trim in the tow condition and self-propulsion conditions with a fixed RPM of 538 are shown in Figure 9 for the three wave conditions. As noted earlier, the towing speeds used in the computations were taken from the self-propulsion speeds obtained for three wave-lengths conditions. The results indicate that the effects of the propeller action on the ship motion are marginal. It is seen that the oscillation amplitudes of the non-dimensional sinkage and trim increase with the wave length and height. Not surprisingly, the ship motion is greatly affected by the wave length and height.

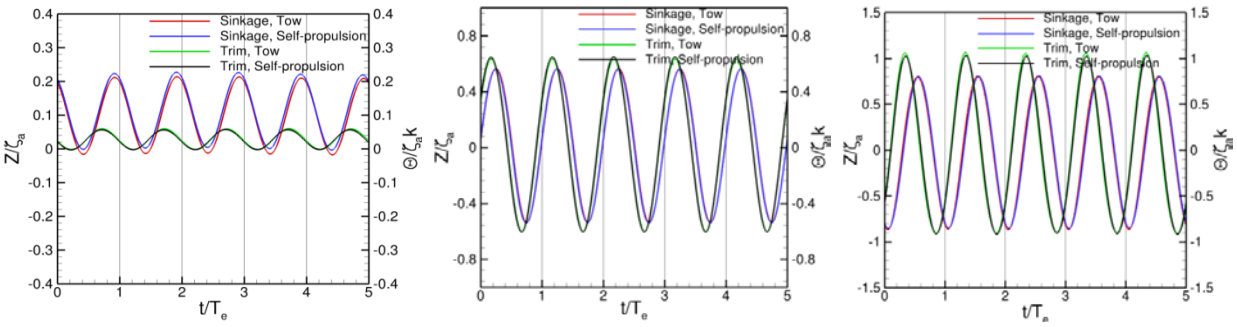

Figure 9: Time histories of the sinkage and trim in tow and self-propulsion conditions in head waves at λ/L=0.5, 1.0, 2.0, h/L=0.02 conditions and fixed propeller RPM of 538

The time-averages of the speed loss, the propeller advance ratio, thrust and torque coefficients are presented in Table 6. As expected, the speed loss is the greatest at the resonance condition (λ/L=1.0). Due to the speed loss (lower ship speed), the advance ratios of the propeller in all wave conditions (computed using ship's speed) are lower than that of the calm water condition with the lowest value occurring at the resonance condition. The propeller thrust and torque are higher in the presence of the waves with the highest value at λ/L=1.0.

Table 6: Time averages of propeller advance ratio, thrust and torque coefficients, and percent change in time-averaged ship speed relative to the calm water condition

	$\bar{J}$	$\bar{k}_T$	$10\bar{k}_Q$	$\Delta\bar{u}$%
Calm water	1.151	0.194	0.06	0
λ/L=0.5	1.105	0.214	0.064	-4.43
λ/L=1.0	0.931	0.306	0.081	-19.46
λ/L=2.0	1.019	0.260	0.073	-12.22

The availability of the hull resistance, propeller thrust, and nominal wake from the computational results allow us to determine the propulsive parameters such as the thrust deduction and hull efficiency, whose variation with the wave length and height is plotted in Figure 10: λ/L=0.0 in this plot represents the calm water condition. The hull resistance and nominal wake-fraction were obtained from separate computations for the towed conditions.

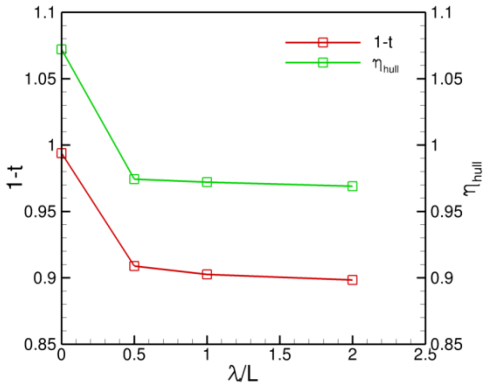

Figure 10: Effects of head waves on thrust deduction factor and hull efficiency at fixed propeller RPM condition

4.2.3 Added Power

In the computations carried out to determine the added power, a PID controller was used to change the propeller RPM in order to maintain the desired ship speed of 1.11m/s (equal to the ship speed for the calm water condition) and therefrom to see how much additional propulsive power will be needed.

Figure 11 shows the comparison of the time histories of the hull axial force (C_{Hull}) and the propeller thrust coefficients (C_T) for three wave conditions. Note that the propeller thrust coefficient here is non-dimensionalized using ship's speed and wetted area in order to make the comparisons with the hull force coefficients meaningful. It is seen that the oscillation amplitudes of both coefficients increase with the wave length and height. While the time-averages of the propeller thrust and hull force should remain in equilibrium in a time-averaged sense, the oscillation amplitude of the hull axial force coefficient, at all wave conditions, is significantly larger than that of the propeller thrust. The oscillation frequencies of both forces are seen to coincide with the wave encounter frequency (T_e). However, there is clearly a phase difference between the two time- histories at all wave conditions, which is presumably due to the complex nature of the forces involved (e.g., added-mass and damping forces on the hull, propeller force). It is worthwhile to remark in passing that the ship's behavior depicted here would also be affected by the parameters selected for the PID controller.

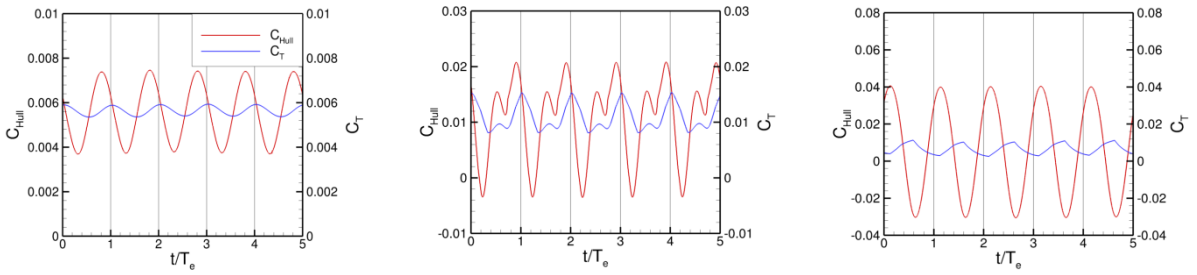

Figure 11: Time histories of the hull axial force and thrust coefficients in regular waves at λ/L=0.5, 1.0 and 2.0, h/L=0.02 conditions and variable propeller RPM

The time histories of the pressure and viscous components of the hull axial force are shown in Figure 12. The oscillation amplitude of the pressure force coefficient is much larger than that of the viscous force, rapidly increasing with the wave length and height. The

oscillation amplitude of the viscous force coefficient peaks at λ/L=1.0 and falls back down at λ/L=2.0. Table 7 summarizes the time-averages of the pressure, viscous and total hull axial force coefficients for the calm water and the wave conditions. The time-averaged pressure force exhibits much larger variation than that of the viscous force coefficient.

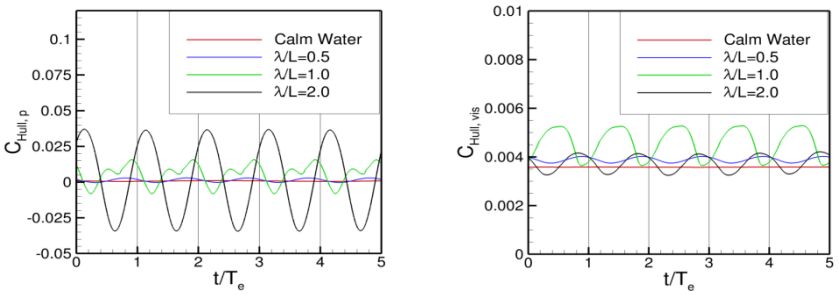

Figure 12: Time histories of non-dimensional pressure and viscous components of axial hull force in regular waves at λ/L=0.5, 1.0 2.0, h/L=0.02 conditions and variable propeller RPM

Table 7: Time averages of non-dimensional pressure and viscous components and total of hull axial force coefficients ($\times 10^3$) at variable propeller RPM

Wave condition	$\overline{C}_{p,hull}$	$\overline{C}_{vis,hull}$	$\overline{C}_{hull}$
Calm water	0.836	3.548	4.384
λ/L=0.5	1.300	3.828	5.128
λ/L=1.0	5.497	4.603	10.100
λ/L=2.0	2.991	3.744	6.735

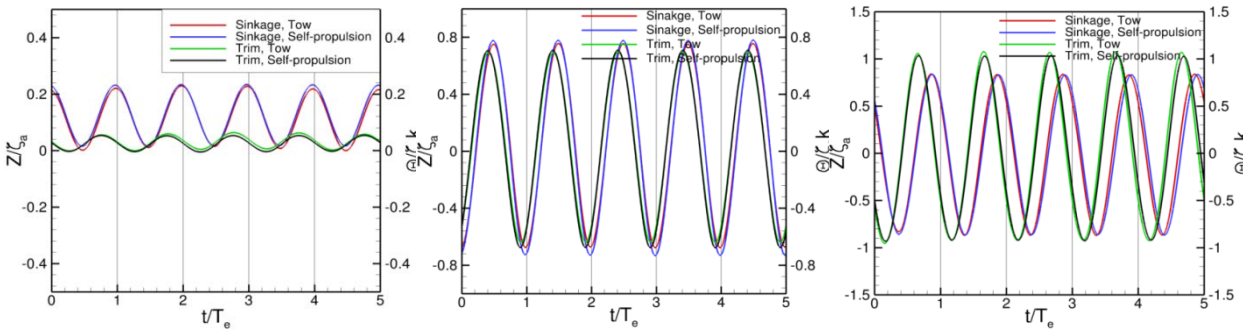

Figure 13: Time histories of sinkage and trim in tow and self-propulsion conditions in regular waves at λ/L=0.5, 1.0 2.0, h/L=0.02 conditions and variable propeller RPM

Figure 13 compares the time history of the non-dimensional sinkage and trim in waves in both the towed and the self-propulsion conditions with variable RPM. It is observed that the propeller action have a marginal effect on the ship motion. The similar conclusion was also drawn for the ship propelled at a constant RPM (see Figure 9). It is also seen that the oscillation amplitudes of both quantities increase with the wave length and height.

Table 8 shows the time-averages of the propeller advance ratio, thrust and torque coefficients, and the percentage change in the propeller RPM and propulsive power required to sustain the ship speed relative to the calm water condition. The propeller operates in a higher loading in waves (lower advance ratio) than in the calm water condition, generating higher thrust and torque. As expected, the highest propeller RPM and propulsive power are

required to maintain the ship speed in the resonance condition (λ/L=1.0). A similar trend was also observed for the propeller running at a constant RPM of 538 (see Table 6).

Table 8: Time averages of propeller advance ratio, thrust and torque coefficients, percent change in propeller RPM and power relative to calm water condition

	$\bar{J}$	$\bar{k}_T$	$10\bar{k}_Q$	$\Delta\overline{RPM}\%$	$\Delta\bar{P}\%$
Calm water	1.151	0.194	0.060	0	0
λ/L=0.5	1.107	0.214	0.064	3.88	20.7
λ/L=1.0	0.940	0.296	0.080	22.18	145.7
λ/L=2.0	1.059	0.24	0.069	7.2	42.6

Figure 14 shows the time-histories of the nominal and the "total" wake fractions in the calm water and the wave conditions. Table 9 summarizes the time averages of the two quantities. Note that the total wake fraction was computed by monitoring a volume-averaged axial flow velocity immediately upstream of the propeller location. As such, it differs from the traditionally defined effective wake fraction. While the time-averaged nominal wake fraction does not noticeably change in presence of waves, its oscillation amplitude seems to increase with the wave length and height most likely due to the effects of the time-varying orbital velocity associated with the regular head waves. The orbital velocity changes its sign (direction) and magnitude in time depending on the axial location of the propeller relative to the wave crests and troughs. It is noteworthy that the total wake-fraction seems to widely vary with the wave length and height, significantly departing from the nominal wake. For the two longer (and larger) waves (λ/L=1.0 and λ/L=2.0), the time-averaged total wake fraction becomes negative, which implies the flow is accelerated enough – by the high propeller loading – to offset the velocity deficit due to the viscous wake.

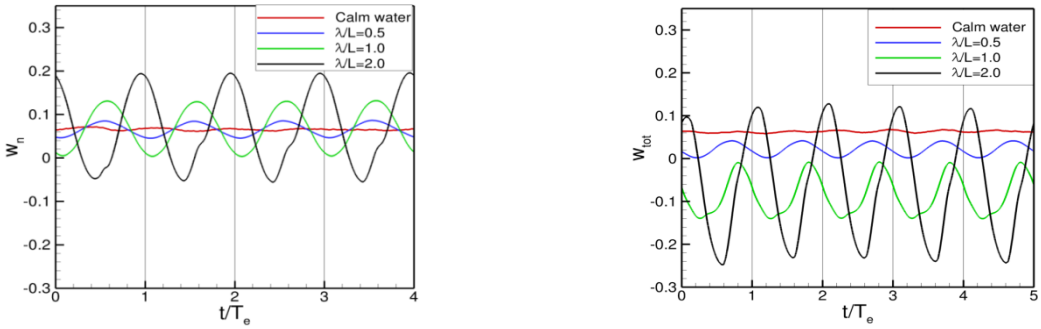

Figure 14: Time histories of nominal (left) and total (right) wake fraction in calm water and regular waves conditions and variable propeller RPM

Table 9: Time average of nominal and total wake fraction at various flow conditions

Wave condition	$\bar{w}_n$	$\bar{w}_{tot}$
Calm water	0.0650	0.064
λ/L=0.5	0.0657	0.021
λ/L=1.0	0.068	-0.084
λ/L=2.0	0.070	-0.066

The variation of the thrust deduction factor and the hull efficiency with the wave length is depicted in Figure 15. Interestingly enough, the hull efficiency has a distinctive minimum at

the resonance condition (λ/L=1.0). This finding is in good contrast to that for the hull efficiency obtained with a constant propeller RPM (Figure 10).

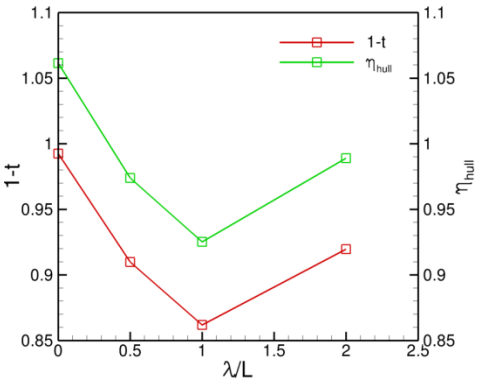

Figure 15: Effects of wave length on thrust deduction factor and hull efficiency at variable propeller RPM condition

5 CONCLUSIONS

- Coupled solutions of two-phase Unsteady Reynolds-Averaged Navier-Stokes equations and six degrees-of-freedom (6-DOF) rigid-body motion (RBM) equations are feasible for predicting the speed loss and added power for a self-propelling ship in regular head sea. We were able to robustly obtain the coupled URANS and 6-DOF RBM solutions for a 1/49 scaled model of the ONR Tumblehome (ONRT) (Model 5613) using unstructured grids.
- The speed loss in regular head seas can be predicted with a commendable accuracy. For the case of λ/L = 1.0 (resonance condition), the coupled URANS/RBM approach can predict the speed loss within 3.0%.
- Coupled solutions of the RANS and 6-DOF rigid-body motion equations allow us to predict not only the added resistance but also the speed loss and added power for a ship cruising in a regular head sea.

AKNOWLEGMENTS

The authors would like to acknowledge support from the Department of Defense (DoD) High Performance Computing Modernization Program (HPCMP) under the Computational Research and Engineering Acquisition Tools and Environments (CREATE) Ship's Hydrodynamics Project, under the direction of Dr. Richard Vogelsong, current HPCMP CREATETM-SH Program Manager.

REFERENCES

[1] The Seakeeping Committee, "Final Report and Recommendations to the 25th ITTC," Proceedings of the 25th ITTC, Vol. 1, Fukuoka, Japan, 2008.
[2] Carrica, P., Wilson, R.V., Noack, R.W. & Stern, F., "Ship Motions Using Single-Phase Level Set with Dynamic Overset Grids," Computers & Fluids, Vol. 36, pp.1415-1433, 2007.
[3] Cura, H. A. and Vogt, M., "Towards the Simulation of Seakeeping and Maneuvering

Based on the Computation of Free Surface Viscous Ship Flow," Proceedings of the 24th Symposium on Naval Hydrodynamics, Fukoka, Japan, 2002.
[4] Simonsen, D. C., Otzen, J. F., Joncquez, S. and Ster, F., "EFD and CFD for KCS Heaving and Pitching in Regular Head Waves," J. Marine Science & Technology, Vol. 18, pp. 435 – 459, 2013.
[5] Sanada, Y., Tanimoto, K., Takagi, K., Toda, Y., and Stern, F., "Trajectories and Local Flow Field Measurements around ONR Tumblehome in Maneuvering Motion," Ocean Engineering, Vol. 72, pp. 45-65, 2013.
[6] Sanada, Y., Elsheikh, H., Toda, Y., and Stern, F., "Effects of Waves on Course Keeping and Maneuvering for Surface Combatant ONR Tumblehome," 30th Symposium on Naval Hydrodynamic, Hobart, Tasmania, Australia, 2-7 November 2014.
[7] Gorski J., Kim S.-E., Aram S., Rhee B., and Shan H., "Development of a CFD Framework for Prognoses of Resistance, Powering, Maneuvering, and Seakeeping of Surface Ships," 30th Symposium of Naval Hydrodynamics, Tasmania, Australia, November 2014.
[8] Shan, H. and Kim, S.-E., "Numerical Study Of Advection Schemes For Interface Capturing In a Volume-Of-Fluid Method On Unstructured Meshes," Proceedings of ASME-JSME-KSME Joint Fluids Engineering Conference, AJK2011-04029, Hamamatsu, JAPAN, July 24-29, 2011.
[9] Kim, S.-E., Rhee, B. and Shan, H., "URANS Simulation of Propeller-Hull Interactions on an Underwater Body," In Proceedings of the 30th Symposium on Naval Hydrodynamics, Pasadena, Hobart, Tasmania, Australia, 2-7 November, 2014.
[10] Ye, H., Shen, Z. and Wan, D., "Numerical prediction of added resistance and vertical ship motions in regular head waves." Journal of Marine Science and Application, Vol. 11, No. 4, pp.410-416, 2012.
[11] Shen, Z. and Korpus, R., "Numerical Simulations of Ship Self-Propulsion and Maneuvering Using Dynamic Overset Grids in OpenFOAM," Presented at the Tokyo 2015 A Workshop on CFD in Ship Hydrodynamics, Tokyo, Japan, 2015.